TiAM kwartalnik naukowo-techniczny
TECHNOLOGIA I AUTOMATYZACJA MONTAŻU
ZESPOŁÓW • MASZYN • URZĄDZEŃ

Monika Lubas[1]

DOI: 10.7862/tiam.2022.4.6

THE VISUAL RESEARCH OF CHANGES IN THE GEOMETRY OF A RIVET JOINT FOR MATERIAL MODEL EFFECT FOR SIMULATION RIVETED JOINTS MADE OF EN AW 5251

BADANIA WIZUALNE ZMIAN GEOMETRII POŁĄCZENIA NITOWEGO NA POTRZEBY OCENY DOBORU MODELU MATERIAŁOWEGO W PRZYPADKU POŁĄCZENIA WYKONANEGO Z EN AW 5251

Abstract

The paper presents the results of a numerical analysis of a single-lap joint with a blind rivet and its geometrical verification by inside views from the experiment. The research aimed to determine how the results of numerical analyses (FEM) were influenced by the method of modeling the material model and how it relates to the experimental results. As part of the analyses, a discrete riveted model and material model: linear and nonlinear were constructed. The analyses took into account various load cases (500, 800, and 900 N) to better illustrate the relationship between the numerical and experimental results. A new methodology of visualizing changes in a riveted joint's geometry was used to validate the results. The technology of making riveted joint cross-sections was developed during a static tensile test. Samples of a single lap joint with blind rivets made of aluminum sheets were subjected to a shear load. Deformations were "frozen" during the test, and sections were prepared. The microscope photos allowed for the development of a method for visualizing the deformation of the hole and rivet. The numerical results (for various loads and various material configurations) were compared with the experimental results of geometric parameters (i.e. angles between sheets or other dimensions) on the riveted joint cross-sections. The obtained results help to understand the mechanism of failure of the blind rivet under load and the complex state of loads in various stages of deformation.

Keywords: blind rivet, numerical analysis, nonlinearity, deformation

Streszczenie

W pracy przedstawiono wyniki analizy numerycznej połączenia zakładkowego z nitem zrywalnym oraz weryfikację geometrii przekrojów połączeń z eksperymentu. Badania miały na celu określenie, jaki wpływ na wyniki analiz numerycznych (MES) ma sposób modelowania modelu materiałowego i jaki ma on związek z wynikami eksperymentalnymi. W ramach analiz skonstruowano model dyskretny połączenia nitowego oraz model materiałowy: liniowy i nieliniowy. W analizach uwzględniono różne przypadki obciążeń (500, 800 i 900 N), aby lepiej zilustrować związek między wynikami numerycznymi a wynikami eksperymentalnymi. Do walidacji wyników zastosowano nową metodologię wizualizacji zmian w geometrii połączenia nitowego. Technologia wykonywania przekrojów połączeń nitowych została opracowana podczas statycznej próby rozciągania. Próbki pojedynczego połączenia zakładkowego z nitami zrywalnymi i arkuszami aluminiowymi poddano testom ścinającym. Odkształcenia zostały „zamrożone" podczas eksperymentu, następnie przygotowano przekroje połączeń. Zdjęcia mikroskopowe pozwoliły na opracowanie metody wizualizacji deformacji otworu i nitu. Wyniki numeryczne (dla różnych obciążeń i różnych konfiguracji materiałów) porównano z wynikami eksperymentalnymi parametrów geometrycznych (tj. kąta między blachami, kąta obrotu nita itd.) na przekrojach połączeń nitowych. Uzyskane wyniki pozwalają zrozumieć mechanizm niszczenia nitu zrywalnego pod obciążeniem oraz złożony stan obciążeń w różnych stadiach odkształcenia.

Słowa kluczowe: nit zrywalny, analiza numeryczna, model nieliniowy, odkształcenia

1. Introduction

Riveted joints are indispensable elements in the design and construction of thin-walled structures and are widely used in many industries [27, 34], including aviation [36]. The most frequently used types of rivets are solid rivets, blind rivets, rivet nuts, and the newly used SPR self-piercing rivets [29]. Most often, solid rivets are used in lap rivet joints, but usually, access from two sides is required when is formed the head. Thin-walled pro-files are connected with blind rivets. The advantages of blind rivets include connection with

[1] MSc. Eng. Monika Lubas, Department of Aerospace Engineering, Faculty of Mechanical Engineering and Aeronautics, Rzeszow University of Technology, al. Powstańców Warszawy 8, 35-959 Rzeszow, Poland, e-mail: m.lubas@prz.edu.pl, ORCID: 0000-0003-1031-7055.

one-sided access, low cost, uncomplicated riveting process, and the possibility of disassembly and reassembly of the joined elements [26, 29]. The geometric parameters, working conditions, and the type of material influence the choice of technology of connection and the type of rivet.

Research on riveted joints was discussed both in experimental and numerical research. The widest group of works are experimental studies of riveted joints. Skorupa [36], carried out an analysis of secondary bending in the lap and overlay riveted joints during the fatigue test. The work [28] described the results of shear tests of joints made with different joining systems. Furthermore, Qasim [33] presented experiments on blind rivets, which concerned the influence of the hole diameter, rivet length, and joint thickness on the shear stresses, mechanical behavior, and in particular the strength. Many authors were focused on the study of static and fatigue tests. In publication [28], the authors presented the results of the experimental analysis of the strength of a single-lap joint in a shear test at 23, 400, 600, and 800°C. They proved that the load capacity of a riveted joint drops drastically with increasing temperature during the static test.

Another author [20] presented the influence of the distance from the rivet to the edge of the sheet on the quality and strength of the joint, and in the article [12] the influence of the configuration of the multilayer joint was examined. The technology of SPR between different combinations of materials has also been investigated experimentally by Jiang et al. [18, 19, 22]. Additionally, in [22], the authors conducted microtopographic observations and hardness measurements and compared the results with P-SPR riveted joints.

The comparison of the experiment with numerical research can be found in many works [3, 16, 25]. The test results indicate that residual stresses and plastic deformation can change the location of the crack initiation and the crack propagation plane.

A separate group of articles [10, 37] was publicized on the research on riveted joints made with the new mechanical method, self-piercing riveting (SPR). Moraes [25] simulated the riveting process using a nonlinear finite element model and the joint deformation process. The authors presented the impact of these processes on the residual stresses and the model of joint failure. Other authors [1, 34] presented results about the fatigue and static strength of cross-shaped SPR joints with aluminum alloy plates at various loading angles.

In many publications, the authors compared the types of connections such as hybrid, adhesive, and riveted joints. Authors [9, 11] presented the experimental results of the geometrical parameters and their influence on the strength. In addition, the results were verified with numerical investigations and shear damage models were also used to model the initiation of the damage in the joints. Furthermore, Pitta [30] presented an experimental and numerical analysis of repairs on carbon fiber-reinforced epoxy (CFRE) substrates, with CFRE and aluminum alloy doublers typical of aircraft structures. In the work [2], the authors described a numerical analysis of a single-lap hybrid (bonded/bolted) composite joint in tension with different load values and different bolt configurations.

The last group of publications of research on riveted joints is works that describe in detail the plastic deformation and changes in the geometry of the joint. In the work [15], the mechanical behavior of a riveted joint with an aluminum rivet under quasi-static load conditions was experimentally investigated and compared with the corresponding tests with the use of a steel rivet. The results of the experiments of the riveting process were then analyzed for the force-displacement curves and the cross-section geometry of the riveted joints. In the next article [14], the cross-sections of riveted joints were used to present the results of tension and shear for different loads. Then the influence of the depth of the die on the energy required before the joint failure and the influence of the rivet hardness on the joint strength were analyzed. Han in his work [13] carried out a microscopic inspection which showed that the quality of the joint was satisfactory despite the increasing level of deformation of the sheet. On the other hand, the article [21] examined two areas of fatigue of riveted aluminum lap joints and T-breaks: mechanisms of crack initiation and development, and the impact of fatigue on joint stiffness. There are many studies on fatigue tests of aircraft components [4-7]. Their approach to determining fatigue data would also be appropriate for aluminum materials used to build riveted joints.

All authors presented excellent work and insight into riveted joint strength investigations and numerical FEM modeling. However, the influence of the material model on the distribution of stresses and deformations was not given. Moreover, the experimental research presented only the results of static and fatigue in the form of graphs.

In this work, a numerical analysis of single-lap blind riveted joints was performed. The aim of the work, the assumption of numerical simulation, was the selection of the material model and modeling of joints and the influence of this model on plastic deformation. The results of the numerical tests were compared with a method of graphical visualization deformation of the rivet and the hole. The new technology allowed making cross-sections of riveted joints during a static

tensile test on a testing machine with different condition loads.

2. Numerical analysis

A numerical experiment was performed on a single-lap riveted joint with a blind rivet configuration using a 3D finite element model created and analyzed in commercial finite element code ANSYS 21R2.

The geometric model used in the analysis was the same as in the case of further experimental research (Figure 1). The riveted joint model was created corresponding to the procedure for tensile shear testing of a single joint (ISO 12996). Moreover, the assumptions were made to reflect the state of axial load in the experimental works.

The mechanical boundary conditions used during the numerical work were as follows:

- Fixed support (all degrees of freedom were fixed) for the left end of the sheet and the left additional surface.
- Allowed displacement (x = free, y = 0, z = 0) at the end of the sheet and right addition-al surface.
- The external load (force F) acts in the x-direction at the right end (Figure 1).

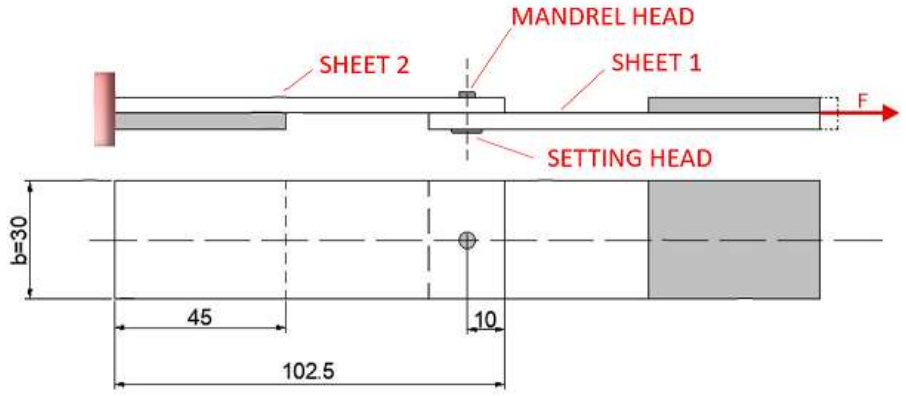

Fig. 1. The geometry of the specimen

The discrete model consists of three solids: a blind rivet and two sheets. The FE mesh contains more than 900 000 elements (tetrahedral elements with 10 nodes) with a quadratic square function – SOLID 187 (Figure 2). The size of the elements and their density was selected through a series of earlier numerical analyzes [23]. In the area of the rivet mandrel, the compaction of the elements was assumed on the contact surface (for more accurate results).

The presented numerical model of the riveted joint was created with the following contact conditions:

- Frictionless contact – sheet-to-sheet,
- Rough contact – sheet(hole)-to-rivet.

The selected contact models were defined based on an earlier series of simulations showing the actual separation of the cooperating elements [23].

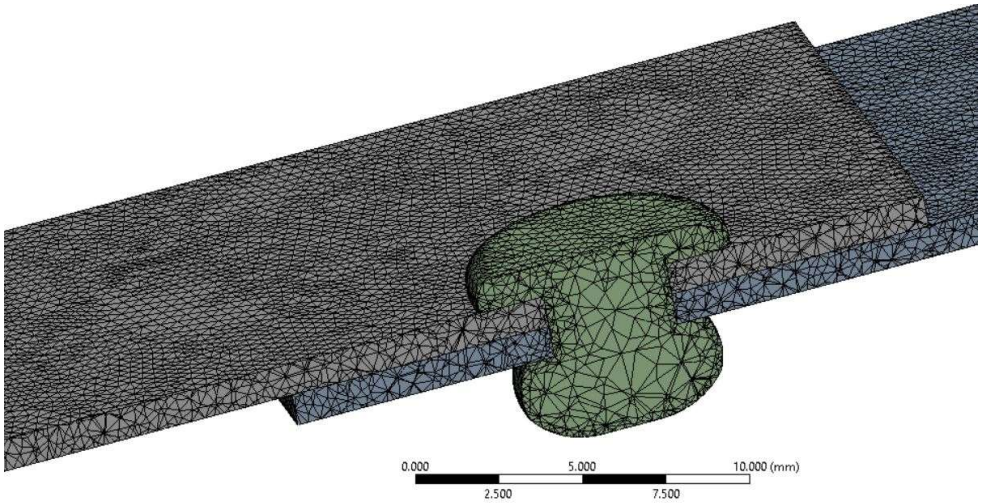

Fig. 2. Mesh riveted joint (cross-section)

The numerical analysis of the riveted joint was tested for two configurations of the material model [23]:

- Only linear elastic material model.
- Both nonlinear (elastic-plastic) models.

The stress-strain curves of the bilinear material model for a sheet and a blind rivet were created and shown in Figure 3. The material properties used to define the material models were presented in Table 1.

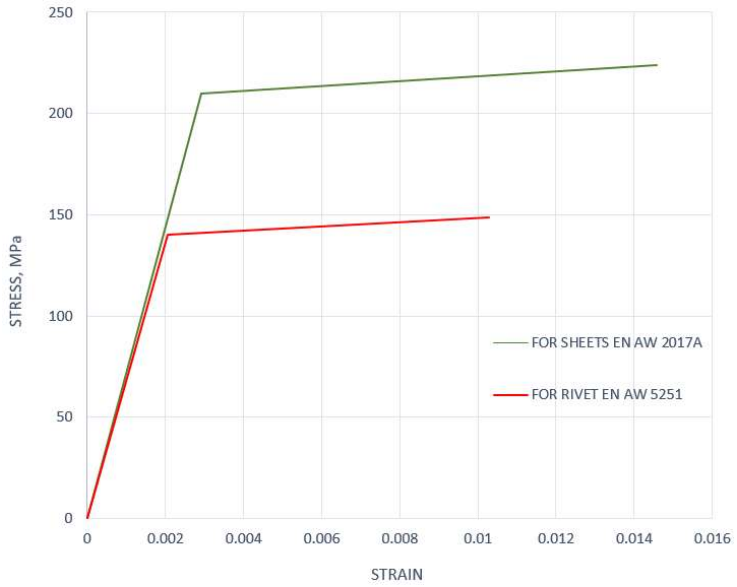

Fig. 3. Stress-strain curve of the bilinear material model for sheets and rivets

Table 1. Mechanical properties of the bilinear material model [31, 32]

Material data	Aluminum alloy EN AW 2017A (sheet)	Aluminum alloy EN AW 5251 (rivet)
Density, kg/mm^3	2700	2700
Young's Modulus, GPa	179	70
Poisson's ratio	0.3	0.3
Yield strength, MPa	288	140
Ultimate tensile strength, MPa	440	240
Tangent modulus, MPa	1200	1000

3. Experimental analysis

3.1. The geometry of joints and materials

For the experimental tests, we used 1 mm thick sheets of aluminum alloy EN AW 2017A. The basic mechanical properties of the sheets and rivets are shown in Table 1.

The prepared samples of sheet metal with dimensions as shown in Figure 1 were connected to EN AW 5251 aluminum alloy blind rivet [32] (diameter of hole 4 mm, length of shank 6 mm, a diameter of shank 4 mm, a diameter of setting head 8 mm) and correspond to the geometry of numerical analysis.

The rivet holes in the sheets were drilled and reamed. 12 samples of a single-lap riveted joint with a blind rivet were made, 4 samples for each load. All riveted joints were made with a pneumatic blind rivet gun with care and the same conditions for making the joint.

3.2. Experimental stand and methodology of measurements

Static tests of riveted joints were performed on a Zwick-Roell Z050 testing machine using Xforce P measuring head with a nominal force Fnom = 20 kN. The increase in the loading force was defined by the constant speed of displacement of the traverse of the machine L = 4 mm/min. Static tests were performed according to ISO 12996 [17].

The shear test was stopped at specific loads:

- F = 500 N,
- F = 800 N,
- F = 900 N.

These values were selected based on the maximum load capacity of 955 N for the riveted joint [24]. The

forces are 50, 80, and 95% of the total strength of the joint. The purpose of stopping the test with different applied loads was to stop further deformation of the joint and "freeze" the deformation state of the rivet. The special equipment was designed to allow the joint area to be flooded with a liquid mixture of polyurethane resin (F19 by Axson) (Figure 4).

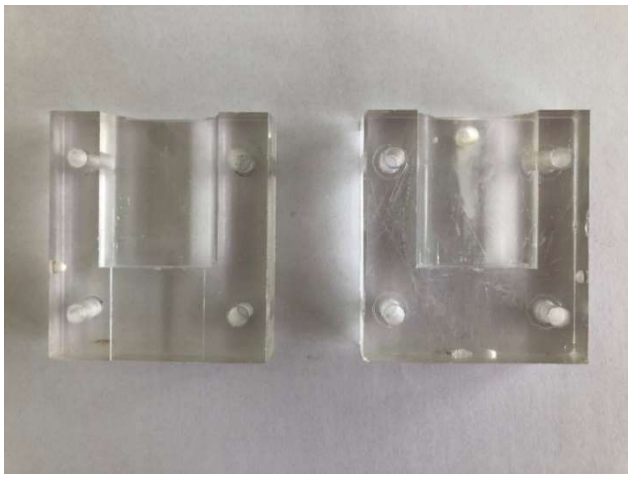

Fig. 4. The geometry of the special device

This device was a bipartite cuboidal form. After the installation of the sample, the was created a closed vessel for the binding mixture, covered the zone of the tested joint (Figure 5). The mold was made of polycarbonate (PC) to enable visual control of the correctness of the pouring process with the binder mixture. The working volume of the vessel was approx. 30 cm^3. After installation on the sample, the mold halves were screwed together with four M6 screws to form a tight seal on the sample. An opening was made in the upper part of the device to allow the liquid mixture to fill it. The adhesive was a polyurethane, two-component (polyol + isocyanate) casting resin F19 by Axson. The basic mechanical properties of the mixture are given in Table 2.

Fig. 5. Installation of the device on the sample

Table 2. Mechanical properties of the mixture [8]

Parameter	Standard	Value
Hardness, Shore D1	ISO 868-85	72
Young's Modulus, MPa	ISO 178-93	1200
Bending durability, MPa	ISO 178-93	50
Compression strength, MPa	ISO 604-93	48
Impact strength Charpy, kJ/m^2	ISO 179/1eU-93	16

Before the test, the working part and the joint area with the rivet were thoroughly cleaned and degreased to obtain the best possible adhesion between the binding mixture and the sample. Next, an anti-adhesive coating was applied to the internal walls of the special tool (form), preventing the device from sticking together permanently and destroying it.

During the static test, a binding mixture amount of 20 cm^3 (life approx. 6-8 minutes at a temperature of 25°C) was prepared. The mixture consisted of polyol and isocyanate in the proportion of 1:1. When the given force is reached, the tensile test was stopped. The mold was placed on the sample (Figure 5) and after obtaining tightness, was filled with the binding mixture using a syringe (Figure 6a). When the mixture was hardened, the deformations of the riveted joint were "frozen" (Figure 6b).

a) b)

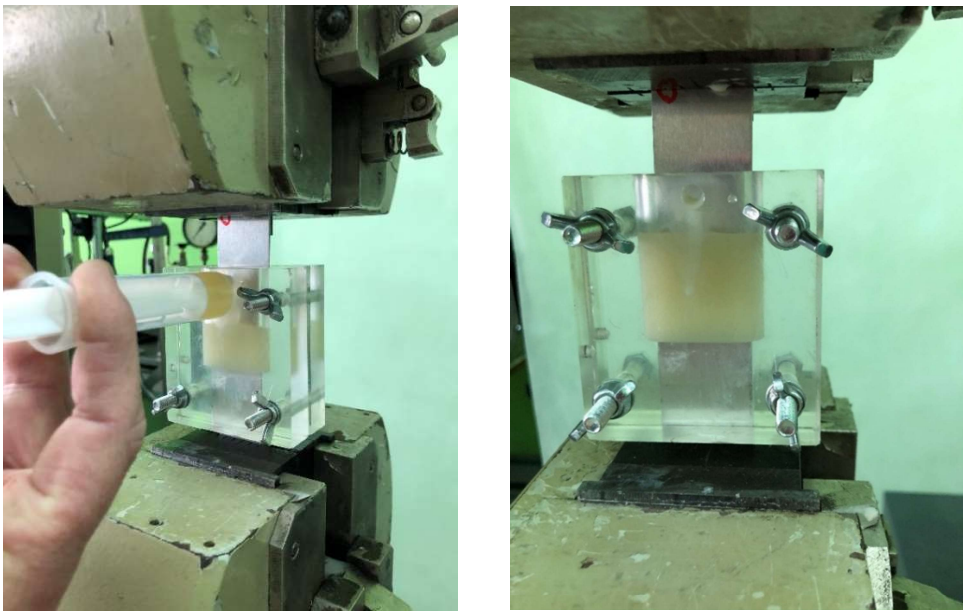

Fig. 6. Filling the device with the binding mixture (a); The sample fixed on the machine during curing (b)

The sample remains fixed on the tensile machine with a stopped load until the mixture reaches the hardening level (for approx. 2 hours). Then the mold was disassembled and the release of the sample was from the handles (Figure 7a). The sample was set aside for min. 24 h to obtain complete hardening of the binder mixture enabling further processing (Figure 7b).

a) b)

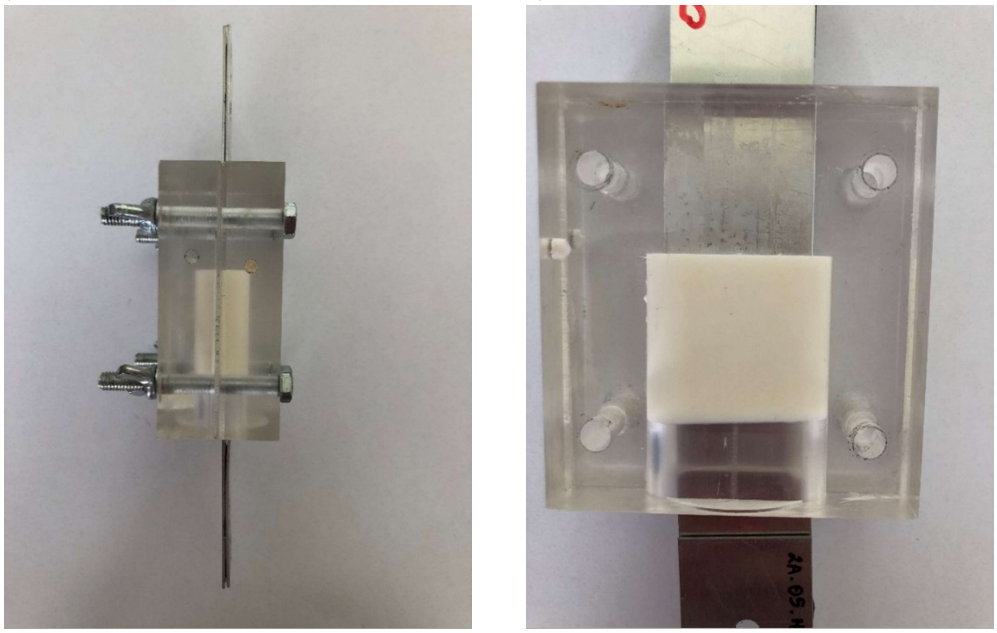

Fig. 7. Disassembling the device from the jaws of the machine (a); "Frozen" deformation of the joint (b)

The next step was to prepare the cross-section of the riveted joint. The sheets outside of the experimental zone were cut off and the sample in it was machined: was milled to 0.2 mm from the longitudinal symmetry plane of the joint, then was ground (<0.2 Ra) within the cross-sectional area.

The sample preparation process carried out in this way enables the optical analysis of the geometric deformation of the riveted joint, in a state close to the real at the moment of the application of the load. The obtained cross-section is then subjected to macro and microscopic analysis using an optical microscope, and

the photos taken allow us to compare and describe the observed changes in the geometry of individual connection elements, i.e. changes in the rivet and hole diameters.

4. Results and analysis

The prepared cross-sections from the numerical analysis and photos from the microscope allowed for the visualization of the deformation state of the riveted joint during the simulation and experiment for the measurement of specific geometrical parameters of the joint.

For the analysis, the following geometrical parameters were defined for the cross-section (Figure 8):

- Rivet deviation angle from the sheet α_1,
- Rivet rotation angle α_2,
- Tangle of sheets separated α_3,
- Diameter of the hole α_4.

The samples of riveted joints were examined for the same forces as were mentioned earlier in Chapter 3.

The definitions of the measured dimensions were presented in Figure 8.

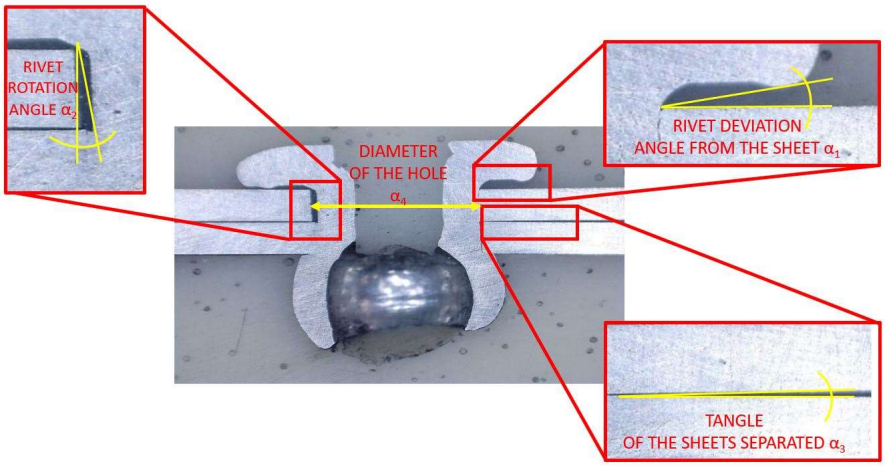

Fig. 8. Defined geometrical parameters of a riveted joint cross-section

The cross-sections made in the experiment were photographed using a microscope and processed for measurement, and some of them are presented in Figures 9-11.

Figure 9 shows the axial cross-section of the joint with a load of 800 N: "a" from numerical analysis and "b" from experimental work. The smallest deformation in the diameter of the hole was observed at $\alpha_4 = 4.03$ mm and a small tangle of sheets separated at $\alpha_3 = 1.42°$. The biggest displacements can be observed for the rivet rotation angle $\alpha_3 = 2.74°$. In the experiment, it was observed that the rivet head formed by the mandrel is visible. At the initial stage of the load (in the linear range of deformation), a slight displacement of the sheets was observed – the angle of the sheets separated $\alpha_3 = 2.27°$ and a small rotation of the rivet, the angle of which was $\alpha_2 = 8.11°$. On the other hand, a greater deviation angle of the rivet from the sheet metal, $\alpha_1 = 11.48°$, and a slight deformation of the hole $\alpha_4 = 4.06$ mm, can be observed.

a)

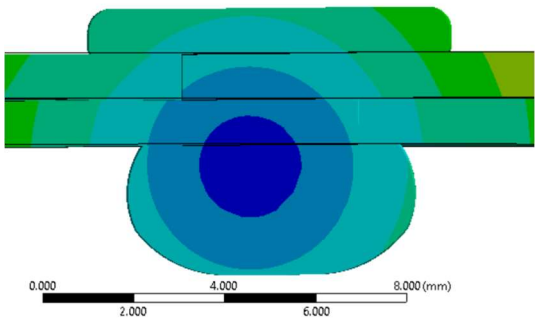

b)

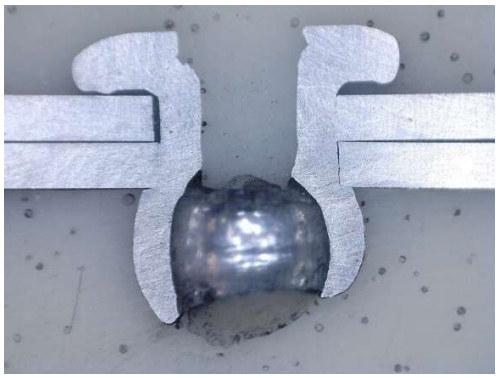

Fig. 9. Cross-section of the joint with load F = 800 N for a linear material model (a); Cross-section of the joint with load F = 800 N (b)

A further increase in the load (up to F = 900 N) causes an increase in deformation, as presented in Figure 10. With the force close to the value of the maximum capacity of the riveted joint, the deformation of the rivet is visible, mainly caused by the shear process. The rivet rotation angle was α_2 = = 23.44°, as the inner cylindrical surface of the rivet (initially smooth) was deformed (displaced and rotated) due to the local high shear stress. Moreover, in the advanced stage of loading, the gap between the joined materials was observed, with the sheet separation angle α_3 = 1.7°. The rivet deviation angle from the sheet was α_1 = 4.76° and was smaller compared to the load in the linear range. The displacement and rotation of the rivet resulted in much greater deformation of the hole and an increase in its diameter with the value of α_4 = 4.19 mm.

Figure 11 shows the axial cross-section of the joint with a load of 900 N: "a" shows the linear material model and "b" is for a nonlinear. The more significant deformation of the joint for the linear material model was observed. The tangle of the sheets separated was α_3 = 1.42° for the nonlinear model, and α_3 = 1.01° for the nonlinear. The rivet rotation angle compared to the nonlinear model was approximately twice as large. On the other hand, the values of the diameters of the hole were similar and comparable to the experiment.

Fig. 10. Cross-section of the joint with load F = 900 N

a)

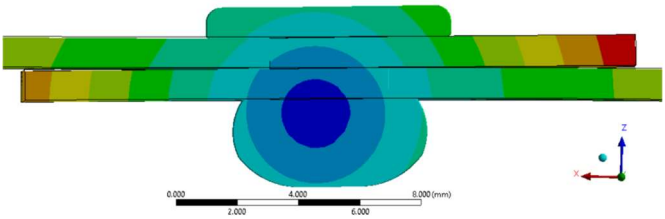

b)

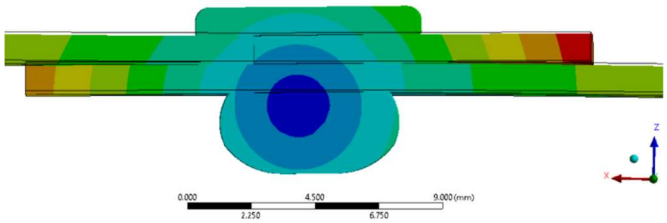

Fig. 11. Cross-section of the joint with load F = 900 N for a linear material model (a); Cross-section of the joint with load F = 900 N for a nonlinear material model (b)

The measured geometrical parameters from the numerical analysis and compared with the experiment work are presented in Table 3.

In the numerical analysis for both material models, the rivet deviation angle from the sheet α_1 having similar values was observed but was a big difference from the experiment. The greatest difference between the numerical analysis and the experiment was in the rivet rotation angle α_2 for a load of 900 N, and with a lower load, the differences were smaller. The smallest differences in numerical analyzes are for the tangle of sheets separated by α_3, up to 800 N, α_3 has higher values for the linear material model and over 900 N for the bilinear. Similar results for each material model were for the diameter of the hole, with slight differences with the experiment.

Table 3. Comparison of geometrical parameters of the riveted joint cross-section

Geometrical parameters	F = 500 N			F = 800 N			F = 900 N		
	Experiment	MES		Experiment	MES		Experiment	MES	
		Linear	Nonlinear		Linear	Nonlinear		Linear	Nonlinear
α_1	2.33°	0.56°	0.28°	11.48°	1.69°	1.43°	4.76°	1.16°	0.94°
α_2	3.55°	2.77°	2.13°	8.11°	2.74°	1.56°	23.44°	2.44°	1.52°
α_3	1.08°	0.87°	0.48°	2.27°	1.42°	1.01°	1.7°	0.82°	1.14°
α_4	4.05 mm	4.01 mm	4.01 mm	4.06 mm	4.03 mm	4.04 mm	4.19 mm	4.05 mm	4.03 mm

The geometrical parameters from the numerical analysis and experiment work were compared in Table 4. For low values of force (500 N) compared to the experimental data, for linear analysis, the greatest difference for the rivet deviation angle from the sheet by 76%, and nonlinear models by 88% were observed. The smallest percentage difference was observed for the diameter of the hole (about 1%). As the load increased, the percentage difference was increased, for the tangle of sheets separated by α_3 in the linear analysis was 20% compared to 500 N. Moreover, significantly changed the rivet rotation angle α_2, the value of which was decreased by more than 40% for both material models.

The opposite situation is for the results for the force of 900 N, compared to the experiment, the most significant difference is for the rivet rotation angle, i.e. a decrease by 89% (linear) and by 94% (non-linear), and the same is accurate for the angle α_1. However, for the tangle of the sheets separated for the linear analysis, the change was 52%, and for the nonlinear analysis by 33%. The smallest changes recorded for the diameter of the hole were 3% and 4%.

The greatest discrepancies in the measured parameters occur for the force of 900 N, and the smallest for 500 N (for α_2 and α_3). For all geometrical parameters of the riveted joint, for all numerical analyses, and only for the diameter of the hole, the differences do not exceed 4%.

Table 4. Percentage comparison of geometrical parameters of the riveted joint cross-section

Geometrical parameters	F = 500 N			F = 800 N			F = 900 N		
	Experiment %	MES		Experiment %	MES		Experiment %	MES	
		Linear %	Nonlinear %		Linear %	Nonlinear %		Linear %	Nonlinear %
α_1	100	24	12	100	15	12	100	24	20
α_2	100	78	60	100	34	19	100	10	6
α_3	100	81	44	100	63	44	100	48	67
α_4	100	99	99	100	99	99	100	97	96

5. Conclusion

In this work, numerical results of blind rivet joints for linear and nonlinear numerical material models were presented. The numerical results were compared with the experiment, with the new methodology of visualizing changes in the geometry of a riveted joint with a blind rivet. Detailed numerical and experimental displacement analysis and plastic deformation analysis were performed on the joint connection.

The results obtained from these investigations lead to the following conclusions:

1. For the lowest examined value of the force (500 N), little differences in deformations are observed in the numerical results, compared to the experimental ones.
2. The method of material modeling did not have a large impact on the value of the geometrical parameters of the joints obtained, estimated by numerical methods. The results closest to the experiment work are obtained from the linear analysis, i.e. the linear material model.
3. Large differences in results are caused by simplifications of the material model (bilinear instead of multilinear), so the plasticization process is not similar to that in the experimental tests.
4. Cross-section analysis with an increase in the destructive force showed a complex state of stress in the rivets, i.e. a combination of shear and bending at an advanced stage of deformation.
5. In the described experiment, the new technology of cross-sections allows the creation of a method of visualizing changes in the geometry of a riveted joint and performing these axial cross-sections under any load of the tensile machine, during various stages of static tests of riveted joints.

The performed numerical analysis and their reference to the experimental data may be the basis for research focusing on the possibility of using simple strength models (bilinear model instead of the multilinear model) in strength analyzes. The analysis could also focus on the linear range of forces and a greater load on riveted joints. The technology and method of visualizing changes in geometry can be used when designing riveted joints with blind rivets. Also, the results obtained help explain the failure of blind rivets. In the future, the prepared cross-sections can be used to calculate the grain size of the alloys for a given load during the static tensile test of the riveted joint.

References

1. Armentani E., Greco A., De Luca A., Sepe R. 2020. „Probabilistic Analysis of Fatigue Behavior of Single Lap Riveted Joints". *Appl. Sci.* 10, 3379.
2. Armentani E., Laiso M., Caputo F., Sepe R. 2018. „Numerical FEM Evaluation for the Structural Behaviour of

a Hybrid (bonded/bolted) Single-lap Composite Joint". *Procedia Struct. Integr.* 8: 137–153.
3. Atzeni E., Ippolito R., Settineri L. 2009. „Experimental and numerical appraisal of self-piercing riveting". *CIRP Annals – Manufacturing Technology* 58: 17–20.
4. Bednarz A. 2020. „Evaluation of Material Data to the Numerical Strain-Life Analysis of the Compressor Blade Subjected to Resonance Vibrations". *Advances in Science and Technology Research Journal* 14, 1.
5. Bednarz A. 2020. „Influence of the Amplitude of Resonance Vibrations on Fatigue Life of a Compressor Blade with Simulated FOD Damage". *Advances in Science and Technology Research Journal* 14,3.
6. Bednarz A., Misiolek W. 2020. „Assessment of the Impact of Shot-Peening on the Fatigue Life of a Compressor Blade Subjected to Resonance Vibrations". *Materials* 12, 5726.
7. Bednarz A., Misiolek W. 2021. „Numerical and Experimental Assessment of the Effect of Residual Stresses on the Fatigue Strength of an Aircraft Blade". *Materials* 14, 5279.
8. BN-89, 6376-02; "Tworzywa Sztuczne; Żywice epoksydowe ; Epidian 1, 2, 3, 4, 5, 6".
9. Bula K., Sterzyński T., Piasecka M., Różański L. 2020. „Deformation Mechanism in Mechanically Coupled Polymer–Metal Hy-brid Joints". *Materials* 13, 2512.
10. Choi D.-H., Han D.-W., Kim H.-K. 2017. „Fatigue life estimation of self-piercing riveted aluminum joints under mixed-mode loading". *Int. J. Fatigue* 97: 20–28.
11. Elzaroug M., Kadioglu F., Demiral M., Saad D. 2018. „Experimental and numerical investigation into strength of bolted, bonded and hybrid single lap joints: Effects of adherend material type and thickness". *Int. J. Adhes. Adhes.* 87: 130–141.
12. Han L., Chrysanthou A., Young K. 2007. „Mechanical behaviour of self-piercing riveted multi-layer joints under different specimen configurations". *Materials and Design* 28: 2024–2033.
13. Han L., Young K.W., Chrysanthou A., Sullivan J.M. 2006. „The effect of pre-straining on the mechanical behaviour of self-piercing riveted aluminium alloy sheets". *Materials and Design* 27: 1108–1113.
14. Haque R., Durandet Y. 2016. „Strength prediction of self-pierce riveted joint in cross-tension and lap-shear". *Materials and Design* 108: 666–678.
15. Hoang N., Porcaro R., Langseth M., Hanssen A. 2010. „Self-piercing riveting connections using aluminium rivets". *International Journal of Solids and Structures* 47: 427–439.
16. Huang L., Guo H., Shi Y., Huang S., Su X. 2017. „Fatigue behavior and modeling of self-piercing riveted joints in aluminum alloy 6111". *International Journal of Fatigue* 100: 274–284.
17. International Organization for Standardization. 2013. „ISO 12996:2013–Mechanical Joining–Destructive Testing of Joints–Specimen Dimensions and Test Procedure for Tensile Shear Testing of Single Joints". *International Organization for Standardization:* Geneva, Switzerland.
18. Jiang H., Luo T., Li G., Zhang X., Cui J. 2017. „Fatigue life assessment of electromagnetic riveted carbon fiber reinforce plastic/aluminum alloy lap joints using Weibull distribution". *International Journal of Fatigue* 105: 180–189.
19. Jiang H.' Sun L., Liang J., Li G., Cui J. 2019. „Shear failure behavior of CFRP/Al and steel/Al electromagnetic self-piercing riveted joints subject to high-speed loading". *Composite Structures* 230, 111500.
20. Li D., Han L., Thornton M., Shergold M. 2012. „Influence of edge distance on quality and static behaviour of self-piercing riveted aluminium joints". *Materials and Design* 43: 22–31.
21. Li D., Han L., Thornton M., Shergold M., Williams G. 2014. „The influence of fatigue on the stiffness and remaining static strength of self-piercing riveted aluminium joints". *Materials and Design* 54: 301–314.
22. Liang J., Jiang H., Zhang J., Wu X., Zhang X., Li G., Cui J. 2019. „Investigations on mechanical properties and microtopography of electromagnetic self-piercing riveted joints with carbon fiber reinforced plastics/aluminum alloy 5052". *Archives of civil and mechanical engineering* 19: 240–250.
23. Lubas M., Bednarz A. 2021. „Material Model Effect for Simulating a Single-Lap Joint with a Blind Rivet". *Materials* 14, 7236.
24. Lubas M., Witek L. 2021. „Influence of Hole Chamfer Size on Strength of Blind Riveted Joints". *Adv. Sci. Technol. Res. J.* 15(2):49–56.
25. Moraes J., Jordon J., Su X., Barkey M., Jiang C., Ilieva E. 2018. „Effect of process deformation history on mechanical performance of AM60B to AA6082 self-pierce riveted joints". *Eng. Fract. Mech.* 209: 92–104.
26. Mucha J. 2017. „Blind Rivet and Plastically Formed Joints Strength Analysis". *Acta Mechanica Slovaca* 21 (1): 62-69.
27. Mucha J., Witkowski W. 2011. „Nośność wybranych rozwiązań połączeń nitowych podczas próby ścinania i rozciągania". *Zeszyty Naukowe Politechniki Rzeszowskiej* 279, 83 (4/11).
28. Mucha J., Witkowski W. 2017. „Analiza wpływu obciążenia termomechanicznego na wytrzymałość połączenia z nitem zrywalnym". *Mechanik* 2, 35.
29. Mucha J., Witkowski W. 2017. „The experimental analysis of the double joint type change effect on the joint destruction process in uniaxial shearing test". *Thin-Walled Structures* 66: 39–49.
30. Pitta S., Roure F., Crespo D., Rojas J.I. 2019. „An Experimental and Numerical Study of Repairs on Composite Substrates with Composite and Aluminum Doublers Using Riveted, Bonded, and Hybrid Joints". *Materials* 12, 2978.
31. Polish Committee for Standardization. PN-EN 485-2+A1:2018-12. 2018. „Aluminium and Aluminium Alloys–Sheet, Strip and Plate–Part 2: Mechanical Properties". *Polish Committee for Standardization:* Warsaw, Poland.
32. Polish Committee for Standardization. PN-EN 573-3:2019-12. 2019. „Aluminium and Aluminium Alloys–Chemical Composition and Form of Wrought Products–Part 3: Chemical Composition and Form of Products". *Polish Committee for Standardization:* Warsaw, Poland.
33. Qasim B., Khidir T. 2021. „Study Strength of Blind Riveted Lap Joint Structure under Tensile Shear Force".

International Journal of Mechanical Engineering and Robotics Research 10, 7.
34. Rao H.M., Kang J., Huff G., Avery K. 2019. „Structural Stress Method to Evaluate Fatigue Properties of Similar and Dissimilar Self-Piercing Riveted Joints". *Metals* 9, 359.
35. Rudawska A., Warda T., Miłosz P. 2015. „Wytrzymałość połączeń klejowych i nitowych". *Technologia i Automatyzacja Montażu* 2: 56-59.
36. Skorupa M., Korbel A., Machniewicz T. 2009. „Analiza wtórnego zginania w mimośrodowych połączeniach nitowych". *Biuletyn WAT* 8, 2.
37. Sun X., Stephens E., Khaleel M. 2007. „Fatigue behaviors of self-piercing rivets joining similar and dissimilar sheet metals". *International Journal of Fatigue* 29: 370–386.